SPATIO-TEMPORAL STRUCTURE OF MIGRATING CHEMOTACTIC BAND OF *ESCHERICHIA COLI*

I. TRAVELING BAND PROFILE

MICHAEL HOLZ AND SOW-HSIN CHEN, *Nuclear Engineering Department, Massachusetts Institute of Technology, Cambridge, Massachusetts 02139 U.S.A.*

ABSTRACT We developed a rapid-scanning, light-scattering densitometer by which extensive measurements of band migration speeds and band profiles of chemotactic bands of *Escherichia coli* in motility buffer both with and without serine have been made. The purpose is to test the applicability of the phenomenological model proposed by Keller and Segel (*J. Theor.* Biol. 1971. **30**:235) and to determine the motility (μ) and chemotactic (δ) coefficients of the bacteria. We extend the previous analytical solution of the simplified Keller-Segel model by taking into account the substrate diffusion which turns out to be significant in the case of oxygen. We demonstrate that unique sets of values of μ and δ can be obtained for various samples at different stages of migration by comparing the numerical solution of the model equation and the experimental data. The rapid-scanning technique also reveals a hitherto unobserved time-dependent fine structure in the bacterial band. We give a qualitative argument to show that the fine structure is an example of the dissipative structure that arises from a nonlinear coupling between the bacterial density and the oxygen concentration gradient. Implications for a further study of the dissipative structure in testing the Keller-Segel model of chemotaxis are briefly discussed.

INTRODUCTION

It has been known since the end of the 19th century(1) that many microorganisms, such as bacteria, show chemotaxis toward oxygen and amino acids. One macroscopic manifestation of such chemotaxis is the gradual formation of a sharp and easily visible band in a cell filled with water when certain amounts of motile bacteria are initially layered in the bottom of the cell. The band migrates slowly upward because the bacteria collectively seek a certain optimum oxygen concentration within a traveling oxygen gradient created by their own metabolism (1). This band formation and migration was effectively used later by Adler (2, 3) in characterizing chemotaxis of E.coli toward various amino acids.

Microscopic motions of individual bacterium in chemotaxis have been studied intensively in the last several years. This has been possible for *Escherichia coli* and *Salmonella typhimurium* by using a tracking microscope (4) and by stroboscopic microphotography (5). The bacteria were subjected to either a spatial gradient (4) or a temporal gradient (5) of an attractant, and the resultant behavior was studied. A combination of these analyses shows (6–8) that the bacterium performs a biased random walk in a region with a spatial gradient,

Reprint requests should be addressed to Professor Chen.

but an isotropic random walk in a region with an homogeneous distribution of attractant. The motion of a bacterium is describable as a continuous alternation between two states: a fairly straight "run" of an average duration, t_1, followed by an uncoordinated tumble or "twiddle" of an average duration, t_2. The twiddle serves to randomize the direction of the next run. The random walk is biased in such a way that when the bacterium is moving in the direction of the positive gradient t_1 is lengthened; on the other hand, when it is moving in the direction of negative gradient t_1 is unaltered. Thus, a bacterium on the time average undergoes a net displacement in the direction of the positive gradient.

In a previous article, (9) we described a light-scattering study of the migrating chemotactic band of *E. coli*. With light scattering techniques, not only can one study the density profile of the band, but also the microscopic motions of bacteria in the band. By analyzing the angular dependence of quasi-elastically scattered light spectrum, we showed that one can obtain microscopic parameters, such as the mean speed (rms speed) of the run, mean jitter speed of the center of mass in the twiddle state, mean step length of the jitter, and most importantly, the ratio $t_1:t_2$. We also studied the migrating band profile, but our comparison with the Keller-Segel (KS) (10) model of the migrating chemotactic band was inconclusive because the diffusion of the substrate—oxygen—was not taken into account.

In this paper we wish to reexamine the problem of migrating band profile more carefully both theoretically and experimentally. Theoretically, we solve the nonlinear KS model equations numerically withtout making an assumption of a vanishing diffusion coefficient of the substrate. We then compare our numerical solution with experimental data to assess (*a*) whether the KS model describes the band profile adequately and, (*b*) if so, whether it gives a unique set of the phenomenological parameters μ (motility coefficient) and δ (chemotactic coefficient). To facilitate the comparison between the numerical solutions and experiments, we employ a moment analysis method, which proves to be an effective way of determining μ and δ. Experimentally, we improve upon our previous method of self scanning of the migrating band through a laser beam. Instead, we construct a rapid-scanning, light-scattering densitometer that allows us to measure a profile in <15 s (as compared to the self-scanning method that takes $\simeq 30$ min) and to do it repetitively and automatically. This rapid scanning not only gives us a more accurate way of measuring the band profile and migration speed, it also reveals a hitherto unobserved time-dependent fine structure of the band.

The band formation is a result of a balance between the random walk of the bacteria, which leads to spreading out of the initially localized bacteria, and the modulation of twiddling frequency by the gradient-sensing mechanism, which tends to bring the bacteria back to a region of optimum substrate concentration. Because the substrate gradient is self-created, the coupling between the bacterial density and the gradient is necessarily highly nonlinear. This nonlinear coupling not only reflects the mechanism of chemotaxis itself, but also makes the study of the band formation and propagation mathematically interesting. We shall not be able to pursue a complete mathematical treatment of these highly nonlinear coupled equations in this paper. Instead, we shall concentrate on a more practical aspect of the problem of determining the phenomenological parameters μ and δ. This reduces the problem to a study of the traveling band profile that corresponds mathematically to the solitary wave solution (11) of the nonlinear equation. In Experimental Procedure we describe the experimental setup, the sample preparation, and the data processing. In Theoretical Analysis we formulate the

theoretical model equations according to the KS (10), taking into account the substrate diffusion, and discuss its traveling band solution. In Discussion, we give results of numerical solutions of the extended KS equation, the moment analysis of the band profile, and comparison between theory and experiment. We then discuss the physical origin of the fine structure. In Conclusions we comment on the usage of the parameter μ extracted from the experiment. We also point out the desirability of further mathematical and experimental studies of the fine structure and the possibility of more stringent tests of the nonlinear coupling term in the KS theory.

EXPERIMENTAL PROCEDURE

Light-Scattering Densitometer

To measure the bacterial density profile in a relatively short time interval, and at the same time being able to capture its fine details, use of a laser beam based densitometer monitoring scattered rather than transmitted light is desirable. The laser beam from a He-Ne laser (operated at 50 mW) can be focused downward into the cell to a diameter of 50 μm, which is much smaller compared to the typical band width of $\simeq$1,000 μm. The scattering intensity is such that a reasonable signal can be obtained in $\simeq$10 s of scanning time through the peak. Our experience is such that although we can clearly see the fine structures of the band in the scattering geometry, such fine details are lost in the transmission geometry. Thus a densitometer such as the one used by Adler (2) would not be able to resolve the fine structures.

Fig. 1 shows a schematic diagram of our densitometer setup. The laser beam is focused gently into the cell C by a lens L_1 (focal length, 10 cm). A motor-driven platform moves the scattering cell up and down with variable speeds of 50–150 μm/s. As the cell starts from an initial position and moves downward, the laser beam is first blocked by a wedge B. The wedge is set at several millimeters below the band position so that at the moment the wedge goes past the laser beam, the light goes through the cell, causing the photocell D to send out a signal to trigger the sweep of a 512 channel Multichannel Analyzer (MCA; model NS-570, Tracor Northern, Middleton, Wisc.). The scattered light is detected at 90° with a lens, L_2 (focal length, 10 cm), that images the band onto the photocathode of a photomultiplier tube (PMT). The output of the PMT is amplified and shaped into logic pulses which are then fed to the input of MCA. The transmitted light, as measured by photocell D, is also recorded on a strip chart recorder. In all the experiments, we find that at the peak of the band $\simeq$85% of the incident laser light is transmitted through the cell. We set the speed of the motor scan and the MCA channel advance time (dwell time $\simeq$70 ms) in such a way that 1 channel of MCA corresponds to $\simeq$7 μm of the scan. The typical count

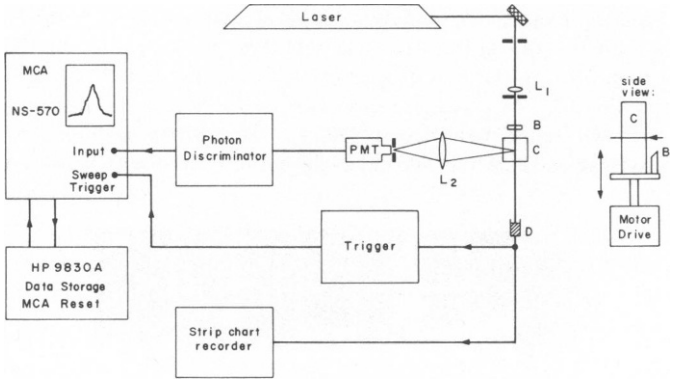

FIGURE 1 The rapid-scanning, light-scattering densitometer with automatic scanning and data recording used in this experiment.

rate of the signal is $\simeq$20,000/s, so that within a dwell time of 70 ms we have a signal of $\simeq$1,400 counts. The scanning is set by the motor control to stop at several millimeters above the band. Then the motor reverses and brings the cell back to the initial position, and a new scan starts again. The MCA is interfaced to a HP-9830/A computer (Hewlett Packard, Fort Collins, Colo.), and the computer manages the data storage and manipulation. As the MCA address advances to the 512th channel, it stops automatically. The computer senses a flag and immediately resets the MCA sweep, so that it is ready to be triggered again. As the scanning motor reverses itself to bring back the cell to its initial position, the computer reads out the data from the MCA memory and stores it on a magnetic tape. A whole cycle takes 50 s to complete. A typical band profile is recorded in $\simeq$150 channels of the MCA, and therefore the scan time through a typical peak is 70 ms/channel $\times$ 150 channels = 10.5 s. An automatic recycle every 50 s, coupled with the locations of successive peaks in the recorded data, allows us to determine the speed of band migration accurately for every 50-s interval. The accuracy of the speed measurement is largely determined by the sharpness of the band profile and the repeatability of the triggering wedge B. The overall accuracy of the speed measurement is $\simeq$10%.

In Fig. 2 we show a sequence of photographs illustrating the formation and the subsequent propagation of the chemotactic band of *E. coli*. The picture to the left was taken 15 min after the inoculation of the bacteria into the bottom of the cell. One clearly sees the formation of a band in the white background which is part of the initial slug left behind. After 59 min, a clear, sharp band begins to pull itself upward, as seen in the middle picture; after 273 min, the band ascends with a speed of $\simeq$0.6 μm/s which can be taken as a propagating solitary wave (11).

Fig. 3 depicts a band shape as measured by our rapid laser beam scanning technique. The lefthand side picture displays the data that were obtained by scanning through the band in $\simeq$10 s. The stage of the band corresponds to approximately the middle picture of Fig. 2. After a curve smoothing by a 7-point averaging, we begin to see some fine structures superposed on the main band profile. This is shown in the middle position of the figure. The fine structure is time dependent, as will be shown later. To obtain the solitary wave profile for a later analysis we can further apply the numerical smoothing to the data. The righthand side picture of Fig. 3 is obtained by applying a 45-point averaging to the data on the lefthand side picture. The result is a smooth curve that can be taken to be the average band profile similar to that obtained by a low resolution densitometer or by our previous self-scanning method.

Sample Preparation

We report here two sets of experiments carried out on consecutive dates, each with *E. coli* bacteria prepared under the same conditions. The same experiment was repeated once and similar results were obtained. A stock solution of wild type *E. coli* K_{12} used in previous experiments (9, 12) was grown in L-broth at 30°C and harvested in late log phase. Details of the growth condition were described in reference 12. The number density of the bacteria (in L-broth) used for inoculation is $\simeq 5 \times 10^8$ bacteria/ml. Two identical rectangular scattering cells of dimension 1 cm^2 (base) $\times$ 5 cm (height) are washed and rinsed with motility buffer (10^{-2} M KH_2PO_4, pH 6.9, 10^{-4} M EDTA, and 10^{-6} M L-methionine) and then filled in the first experiment with motility buffer only and in the other with motility buffer containing 10^{-2} M L-serine. In the second experiment the cells are filled, respectively, with 10^{-2} M and 10^{-3} M L-serine. In each case 200 μl of the cultured medium are freshly drawn from the test tube with a syringe and carefully layered at the bottom of the cells, which are left open to air at

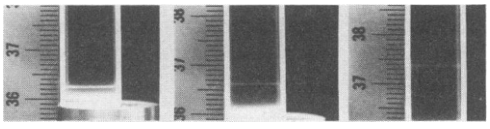

FIGURE 2 A sequence of photographs of a migrating chemotactic band in a rectangular cell containing motility buffer. The pictures (from left to right) are taken at 15, 59, and 273 min, respectively, after the bottom of the cell is inoculated with bacteria. Average speed of migration between consecutive pictures is 1.4 and 0.6 μm/s, respectively. (Linear scale is in centimeters.)

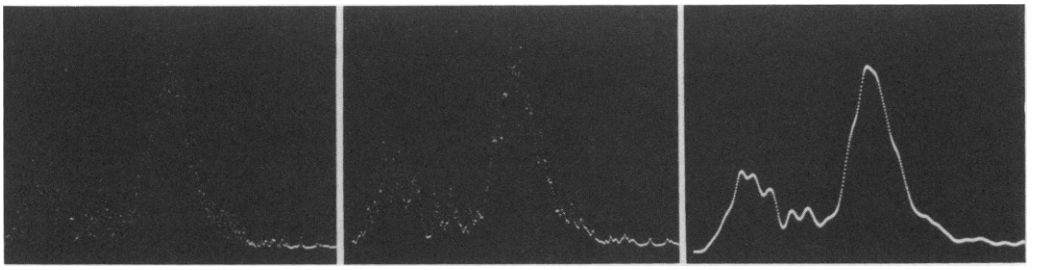

FIGURE 3 The band shape as measured by the rapid laser beam scanning technique (scanning time, 10 s). The oscilloscope picture on the left is the original data. The pictures in the center and on the right are results of a 7-point and a 45-point averaging applied to the original data (see text for explanation of the curve smoothing procedure). The prominent peak on the right is the migrating chemotactic band as it begins to move away from part of the initial slug of bacteria seen on the left.

all times. The number of bacteria injected is estimated to be $\simeq 1 \times 10^8$. As shown in Fig. 2, the band formation starts at $\simeq$15 min after inoculation. During the experiment the two scattering cells are measured alternately.

We also inoculated cells containing motility buffer and 10^{-4} M L-serine. In these cases the band appears quickly but is very broad ($\simeq$5 mm wide) and the density of bacteria in the band is so low that the signal obtained is too weak to be measured with our rapid scanning densitometer.

Data Processing

As mentioned in the last subsection, an estimate of the band migration speed is conveniently obtained by measuring the positions of successive peaks recorded, each taken at a constant interval of 50 s. Because the band profile contains fine structures, the precision of the band speed measurement also depends on the accuracy for locating the center of the peak. In each measurement (a subset of an experiment) the band profile is measured 10 consecutive times. For each recorded profile $B(\xi)$ we compute its first moment $<\xi>$ (see Theoretical Analysis for the notation). We thus have 10 first moments from which we can take the differences among them to calculate the average speed within a $50 \times 9 = 450$ s interval. We generally find that within $\simeq$10 min the band speed does not fluctuate more than $\pm$ 10%. However, over a time interval of 1 h the speed can change appreciably.

For comparison with the theoretically calculated band profiles we have to smooth out the fine structure from the measured data. Fortunately, the fine structure has a much narrower band width than the solitary wave profile. We can therefore use the technique of numerical filtering, as was illustrated in Fig. 3. We employ a 7-point (1 ± 3 adjacent points) or a 45-point (1 ± 22 adjacent points) averaging with a truncated Gaussian weighting function. The 7-point averaging is used to bring out the fine structure from the raw data and the 45-point averaging is used to smooth out the fine structure to obtain the solitary wave profile. This procedure works consistently well for all data we have taken.

THEORETICAL ANALYSIS

KS Model (10)

Two variables of interest in the migrating band problem are: (*a*) $b(z, t)\, dz$, the number of bacteria per unit area between heights $(z, z + dz)$ at time t and (*b*) $c(z, t)\, dz$, the number of substrate molecules per unit area between heights $(z, z + dz)$ at time t. The continuity equation expressing the conservation of the number of bacteria is then

$$\frac{\partial b}{\partial t} = -\frac{\partial}{\partial z}\left[-\mu \frac{\partial b}{\partial z} + v_c b\right] \tag{1}$$

The first term in the bracket on the righthand side of the equation expresses the diffusion current in the z-direction due to the random motion. This can be taken as a macroscopic manifestation of the microscopic random walk. This random walk is, however, biased toward the positive z-direction by the presence of the second term, which is the effective chemotactic current in the z-direction. If the chemotactic speed v_c were a constant, then Eq. 1 is nothing but a Fokker-Planck equation derivable from the Langevin equation of a particle in an external field. The solution of (1) would then be a band propagating in the z-direction with a speed v_c (13). However, the situation is more complicated due to the fact that the chemotaxis is a result of the gradient-dependent modulation of the frequency of twiddles, as mentioned in the introduction. As a result, v_c is a function of the substrate concentration $c(z, t)$. This functional dependence is postulated by KS to be of the form

$$v_c(c) = \frac{\delta}{c}\frac{\partial c}{\partial z}. \tag{2}$$

v_c is thus proportional to a logarithmic derivative of the substrate concentration, and δ is called the chemotactic coefficient. This form of the chemotactic current was shown to be reasonable by Dahlquist et al. (14) in an experiment done with controlled substrate gradients. The singular form of $v_c(c)$ was further shown (10) to be necessary for KS equations to produce a traveling wave solution.

The corresponding conservation equation for $c(z, t)$ is also easily written down as

$$\frac{\partial c}{\partial t} = -\frac{\partial}{\partial z}\left[-D\frac{\partial c}{\partial z}\right] - kb, \tag{3}$$

where D is the diffusion coefficient of the substrate in water, and k is the number of substrate molecules consumed per second per bacterium. The second term on the righthand side thus expresses a constant rate of consumption of substrate by the bacteria. This assumption was shown to be valid for not-too-low concentration of the substrate by Adler (3).

As can be seen from Fig. 2, the bacteria form a sharp band and because the band propagates at an approximately constant speed over a limited length of time (10 min, which is much longer than our measurement time), it is useful to make a transformation of the coordinate to a moving frame defined by

$$\xi = z - \bar{v}t; \qquad \tau = t. \tag{4}$$

This transformation amounts to replacements:

$$\frac{\partial}{\partial t} \to \frac{\partial}{\partial \tau} - \bar{v}\frac{\partial}{\partial \xi}; \qquad \frac{\partial}{\partial z} \to \frac{\partial}{\partial \xi}, \tag{5}$$

and Eqs. 1, 2, and 3 become

$$\frac{\partial b}{\partial \tau} - \bar{v}\frac{\partial b}{\partial \xi} = \mu\frac{\partial^2 b}{\partial \xi^2} - \frac{\partial}{\partial \xi}\left(\frac{\delta}{c}\frac{\partial c}{\partial \xi}b\right) \tag{6}$$

$$\frac{\partial c}{\partial \tau} - \bar{v}\frac{\partial c}{\partial \xi} = D\frac{\partial^2 c}{\partial \xi^2} - kb. \tag{7}$$

This is a set of coupled nonlinear partial differential equations, and the solution of it, with

appropriate boundary and initial conditions, should give rise to both the band formation (initial stage, such as the lefthand side picture of Fig. 2) and band propagation (final stage, such as the righthand side picture of Fig. 2). In general, numerical techniques have to be used for solution of such equations. The initial band formation stage has been studied numerically by Scribner et al. (15). We are more interested in the final stage of band propagation here. In their study of this problem, KS (10) neglected the τ dependence of $b(\xi, \tau)$ and $c(\xi, \tau)$ from the very beginning. Strictly speaking, this is not allowed. This is evidenced by looking at Fig. 3 where we showed time varying fine structures superposed on an average band profile. This suggests that $b(\xi, \tau)$ and $c(\xi, \tau)$ can be written as

$$b(\xi, \tau) = B(\xi) + b'(\xi, \tau)$$

and

$$c(\xi, \tau) = C(\xi) + c'(\xi, \tau), \tag{8}$$

each of which consists of a time-independent stationary band profile and a time-dependent perturbation superposed on it. If the perturbations are much smaller, compared to the overall band profile, and furthermore if the time average $\overline{b'(\xi, \tau)} = \overline{c'(\xi, \tau)} = 0$, then by substituting Eq. 8 into 6 and 7, and linearizing them, we get a set of coupled ordinary differential equations for the average band profile $B(\xi)$ and $C(\xi)$, as originally given by KS:

$$-\bar{v}\frac{dB}{d\xi} = \mu\frac{d^2B}{d\xi^2} - \frac{d}{d\xi}\left(\frac{\delta}{C}\frac{dC}{d\xi}B\right) \tag{9}$$

$$-\bar{v}\frac{dC}{d\xi} = D\frac{d^2C}{d\xi^2} - kB \tag{10}$$

To obtain $B(\xi)$ from the experimental profile, such as in Fig. 3, we can do it two ways: time average $b(\xi,\tau)$ and assume (plausibly) $\overline{b'(\xi, \tau)} = 0$. This corresponds to our old method of self scanning. Because of the long time taken for the self scanning ($\simeq$30 min as compared to the characteristic fluctuation time of $b'[\xi, \tau]$ of the order of 10 s) to complete, the experiment essentially measures $B(\xi)$; or ensemble averge $b(\xi, \tau)$ by superposing many $b(\xi, \tau)$ profiles, each measured at 50-s intervals. An alternative way of achieving an approximate ensemble averaging, is to smooth out the measured profile by applying a numerical filtering as was mentioned in the last section.

This procedure of linearizing Eqs. 6 and 7 to obtain Eqs. 9 and 10 is justified only when the fluctuations b' and c' are indeed small. Under certain circumstances the fluctuations can be so large that the linearized equations are different from Eqs. 9 and 10 because it would contain renormalized terms. We shall not discuss this case in this article. Obviously, the KS Eqs. 9 and 10, which give only the so-called solitary wave solution (11, 16) of the original Eqs. 6 and 7, do not exhaust all the interesting features of the propagating band.

The Solitary Wave Equation

We shall solve Eqs. 9 and 10 under the following boundary conditions:

$$\text{at } \xi = -L, \qquad C = 0, \frac{dC}{d\xi} = 0; \tag{11}$$

$$\text{at } \xi = +L, \qquad C = C_0; \tag{12}$$

and

$$\text{at } \xi = \pm L, \qquad \frac{dB}{d\xi} = B = 0. \tag{13}$$

Condition in Eq. 11 means the bottom of the cell is closed and the bacteria consume all the substrate molecules as they pass by; this fact was indicated in Adler's experiments (2). Condition in Eq. 12 means that the cell is open to air on the top, and the solution has a saturated oxygen concentration, C_o, there. Actually this condition is not curcial, as it turns out, because in the experiments the band is always sufficiently far from the top so as never to disturb the oxygen concentration there. Condition in Eq. 13 is valid, because experiments show that the bacteria are highly concentrated on a narrow band. Under these conditions, Eq. 9 can be easily integrated (15) to give

$$B(x) = Re^{-x}[C(x)]^{\bar{\delta}}, \tag{14}$$

where we introduce reduced quantities

$$x = \frac{\bar{v}}{\mu}\xi \tag{15}$$

and

$$\bar{\delta} = \frac{\delta}{\mu}, \tag{16}$$

and R is the constant of the integration to be determined later. Eq. 14 is a rigorous consequence of Eq. 9 and the boundary conditions. The exponential factor guarantees a rapid decay of the band profile $B(x)$ for large x. On the other hand, for the negative values of x, the substrate concentration $C(x)$ decays sufficiently fast to also guarantee a rapid decay of $B(x)$. We note that the value of $\delta > 1$ would also enhance this decay. Eq. 14 indicated that the bacterial distribution peaks at the point where the logarithmic derivative of $C(x)$ is equal to $1/\bar{\delta}$, i.e.,

$$\frac{d}{dx} ln\, C(x)\big|_{x=x_m} = \frac{1}{\delta}. \tag{17}$$

To find $C(x)$, we come back to Eq. 10. First, we can find out the speed of migration by integrating both sides from $-L$ to L to get

$$-\bar{v}C_0 = -k\int_{-L}^{L} d\xi B(\xi) + D\frac{dC}{d\xi}\Big|_{-L}^{L}. \tag{18}$$

Denoting the inside area of the cell by A and the total number of bacteria by N, we can then, from Eq. 18, solve for the speed

$$\bar{v} = \frac{kN}{AC_0} - \frac{D}{C_0}\frac{dC}{d\xi}\Big|_L. \tag{19}$$

We see from this expression that the band propagation speed is determined primarily by the rate of consumption of the substrate by the bacteria (first term). This rate is reduce slightly by

the downward diffusion of the substrate (second term). The numerical estimate shows that the second term amounts to <15% of the first term for oxygen. Therefore the study of migration speed offers very little information other than the substrate consumption rate k, which could probably be measured more easily by other means. We shall see, however, that the width of the band gives many more interesting parameters.

Next we substitute Eq. 14 into Eq. 10 and rewrite it in terms of reduced quantities

$$f = \frac{C}{C_0} \tag{20}$$

and

$$\gamma = \frac{\mu}{D} \tag{21}$$

to get

$$\frac{d^2f}{dx^2} + \gamma \frac{df}{dx} = Qe^{-x} f^{\bar{\delta}}, \tag{22}$$

where Q is a constant derivable from R, i.e.,

$$Q = \frac{k\mu^2}{D\bar{v}^2} R C_0^{\bar{\delta}-1} \tag{23}$$

The KS (10) analytical solution was obtained by setting $D \to O$ or $\gamma \to \infty$, so that the first term of Eq. 22 can be neglected compared to the second term. To determine the constant Q, we demand from Eq. 14 that an integral of $B(x)$ over all x gives the total number of bacteria N. We then substitute the R, so obtained, into Eq. 23 to get

$$Q \int_{-L}^{L} dx e^{-x} f(x) = \frac{k\mu}{D\bar{v}C_0} \frac{N}{A}. \tag{24}$$

We can further assume $\bar{v} \simeq kN/AC_0$ from Eq. 19, because the band is so far away from the top of the tube that $dc/d\xi$ at L is very small. Then, from Eq. 24, we obtain

$$Q = \gamma \left[\int_{-L}^{L} dx e^{-x} f^{\bar{\delta}}(x) \right]^{-1} \tag{25}$$

Using this expression of Q in Eq. 22, with the first term neglected, we obtain the KS analytic solution

$$f_{KS}(x) = [1 + e^{-x}]^{-1/(\bar{\delta}-1)}. \tag{26}$$

In the case of oxygen substrate, $D = 2 \times 10^{-5}$ cm^2/s (17) and a typical motility coefficient is $\mu \simeq 1 \times 10^{-6}$ cm^2/s, so that $\gamma \simeq 0.05$. Under this circumstance, neglect of the first term in Eq. 22 is completely unjustified. We therfore have to solve Eq. 22 numerically for different sets of parameters γ and $\bar{\delta}$. By applying a transformation $x \to x - x_0$, we can easily see that different values of Q merely correspond to different choices of the origin x_o. Because experimentally we always choose the origin to be at the center of the peak of $B(x)$, the precise value of Q is irrelevant. It is already obvious from the KS solution that by studying the line

shape of $f(x)$, or equivalently $B(x)$, one can get values of $\bar{\delta}$ and μ. We shall describe the method of numerical solution of Eq. 22 and its results in the following section.

DISCUSSION

Numerical Solution of Eq. 22

To solve Eq. 22 by a standard finite difference method (18), we linearize the nonlinear term on the righthand side as follows. Let

$$f = f_0 + \Delta f, \tag{27}$$

where f_o is the zeroth order solution of the equation obtained initially by a guess. Then

$$\begin{aligned} f^{\bar{\delta}} &= (f_0 + \Delta f)^{\bar{\delta}} \\ &\doteq f_0^{\bar{\delta}} + \bar{\delta} f_0^{\bar{\delta}-1}(f - f_0) \\ &= f_0^{\bar{\delta}}(1 - \bar{\delta}) + \bar{\delta} f_0^{\bar{\delta}-1} f \end{aligned} \tag{28}$$

Therefore we can rewrite Eq. 22 as

$$\frac{d^2 f}{dx^2} + \gamma \frac{df}{dx} - \bar{\delta} f_0^{\bar{\delta}-1} f = f_0^{\bar{\delta}}(1 - \bar{\delta}), \tag{29}$$

which is a linear equation, and the standard iteration technique can be applied. We solve Eq. 29 in an interval from L_1 to L_2, i.e., $L_1 = -30 \leq x \leq 180 = L_2$ with a boundary condition

$$f(L_1) = 0, \qquad f(L_2) = 1, \tag{30}$$

which is reasonable for such a large interval. Eq. 29 is solved for an initial guess of $f_0 = 1$, $L_1 \leq x \leq L_2$, and the $f_1(x)$ so obtained, is substituted back as a new f_0 in the equation. An improved solution $f_2(x)$ is then obtained. This iteration continues until

$$| f_k(x) - f_{k-1}(x) | \leq \epsilon, \tag{31}$$

where ϵ is generally set at 10^{-3}, and the number of iterations is typically $\simeq 30$. The solution is stable, in the sense that it is quite insensitive to the initial guess of $f_o(x)$. In fact, if we take $f_o(x)$ to be $f_{KS}(x)$, the iteration converges similarly.

The finite difference equation is generally solved twice. The first time we use the large interval $-30 \leq x \leq 180$ with the grid size $\Delta x = 1.0$ and boundary condition (Eq. 30). After it converges, we then resolve it in a smaller interval, $l_1 \leq x \leq l_2$, with a finer grid size, $\Delta x = 0.1$, but with the boundary condition at l_1 and l_2 taken from the first solution. In the second solution, we can also impose a smaller error ϵ such as 10^{-5}.

Fig. 4 shows a solution of Eq. 22 and the corresponding $B(x)/B_{max}$ for the case $\gamma = 0.05$ and $\bar{\delta} = 2.0$. The corresponding KS analytical solution is also displayed for comparison. We note while $f(x)$ shows a great deal of difference because of diffusion, the difference in the bacterial density profiles is not as pronounced. This is because of the presence of an exponential factor in Eq. 14. Notice also that in KS solution the peak of $B(x)$ always occurs at $f = 0.5$ point, but in our numerical solution it occurs at a point defined by Eq. 17, which is generally at x_m where $f(x_m) < 0.5$.

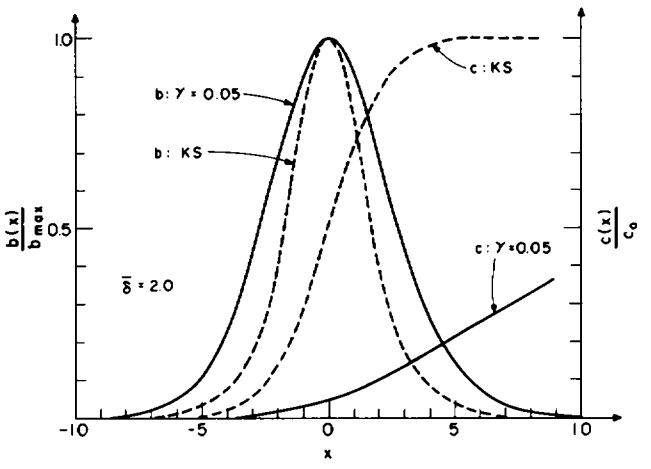

FIGURE 4 Comparison of the bacterial density (b) and the substrate concentration (c) distribution as predicted by the Keller-Segel (KS) analytical solution and our numerical solution incorporating the substrate diffusion. The chemotactic strength parameter $\bar{\delta} \equiv \delta/\mu$ is fixed at 2.0 for both cases. $\gamma \equiv \mu$:D is the ratio between the bacterial motility coefficient and the diffusion coefficient of the substrate. It is to be noted that although the substrate diffusion has a drastic effect on the concentration distribution, the effect on the bacterial density distribution is considerably reduced (see text for explanation).

Moment Analysis of the Density Profile

For the sake of a speedy comparison between theoretical and experimental profiles, we choose to compare their moments. We are only interested in extracting two parameters μ and $\bar{\delta}$ from the experiment, and it is sufficient to compare two or three integrated quantities. If we have a distribution $F(x)$, we can calculate its moments $\langle x^n \rangle$ for $n = 0, 1, 2, 3, \ldots$ We can easily verify the following useful properities of the moments: (a) The zeroth moment, or the area under $F(x)$, does not change even if we measure $F(x)$ with a finite spatial resolution (such as a finite width of laser beam). (b) To first order in the resolution, the first moment $\langle x \rangle$ is not affected by the spatial resolution. (c) If we denote the spatial resolution by Δ (i.e., the width of

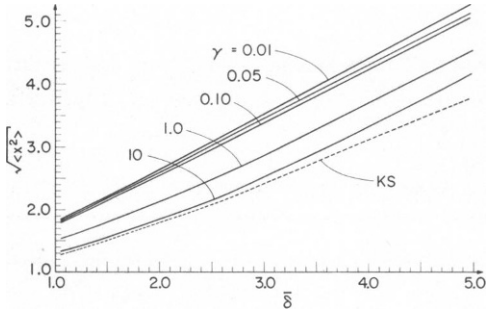

FIGURE 5

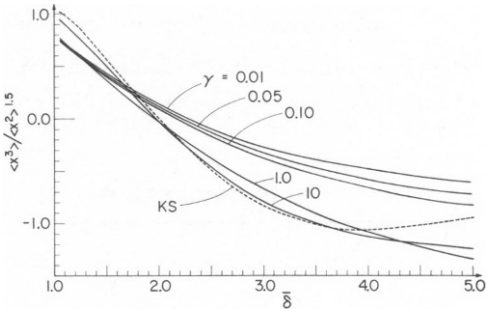

FIGURE 6

FIGURE 5 $\bar{\delta}$ and γ dependence of the dimensionless width of the band. The width is defined as the root mean square of the second central moment of the bacterial density distribution.

FIGURE 6 $\bar{\delta}$ and γ dependence of the normalized third central moment of the bacterial density distribution. Note that this quantity changes sign around $\bar{\delta} = 2.0$.

TABLE I
DEPENDENCE OF RMS-WIDTH $\sqrt{\langle x^2 \rangle}$ ON PARAMETERS γ AND $\bar{\delta}$

γ	$\bar{\delta}$					
	1.1	1.5	2.0	2.5	3.0	5.0
0.05	1.86	2.19	2.61	3.03	3.46	5.14
0.10	1.83	2.14	2.55	2.96	3.39	5.07
1.00	1.57	1.80	2.13	2.48	2.86	4.56
10.0	1.36	1.56	1.86	2.21	2.54	4.19
KS	1.31	1.51	1.81	2.16	2.46	3.69

The Keller-Segel model is equivalent to $\gamma \geq 100$.

the laser beam), the measured second moment is broadened by a fraction, $\Delta^2/12 \langle x^2 \rangle$, which is negligible in our experiments. (*d*) Corrections to the $\langle x^3 \rangle$ and $\langle x^4 \rangle$ are similarly small.

As we mentioned earlier, we always take the peak to be at the origin; this is equivalent to using only the central moments, i.e., $\langle (x - \bar{x})^n \rangle$. $\bar{x} \equiv \langle x \rangle$, taken from the experimental data, was already used to measure the band propagation speed.

In Fig. 5, we plot the square root of the second central moment as a function of $\bar{\delta}$ for different γ values. We see that our numerical results approach KS results only when $\gamma > 10$. In a typical range of interest where $\gamma \simeq 0.05$, the difference between KS and our result is quite substantial. This shows that diffusion of the substrate, such as oxygen, cannot be neglected.

In Fig. 6 we plot the normalized third central moment as a function of $\bar{\delta}$ for the same set of γ values. An interesting feature is that this quantity changes sign at approximately $\bar{\delta} \simeq 2.0$ (which is exact for the KS solution). Thus the third central moment is useful in characterizing asymmetry of the band profile.

Tables I and II list some numerical values of these calculated moments, which can be used to reconstruct Figs. 5 and 6. Furthermore, Table III also lists the calculated normalized fourth central moments.

Comparison of Theory and Experiments

The main results of the experiment are summarized in Tables IV and V. Table IV lists results of two experiments performed on the same day; one with oxygen-saturated motility buffer

TABLE II
DEPENDENCE OF $\langle x^3 \rangle / \langle x^2 \rangle^{1.5}$ ON PARAMETERS γ AND $\bar{\delta}$

γ	$\bar{\delta}$					
	1.1	1.5	2.0	2.5	3.0	5.0
0.05	0.70	0.41	0.11	−0.14	−0.33	−0.70
0.10	0.70	0.40	0.09	−0.16	−0.38	−0.82
1.00	0.72	0.37	−0.03	−0.38	−0.67	−1.33
10.0	0.90	0.50	−0.03	−0.46	−0.79	−1.23
KS	0.99	0.57	0.00	−0.50	−0.83	−0.92

TABLE III
DEPENDENCE OF $\langle x^4\rangle/\langle x^2\rangle^2$ ON PARAMETERS γ AND $\bar{\delta}$

γ	$\bar{\delta}$					
	1.1	1.5	2.0	2.5	3.0	5.0
0.05	1.30	1.18	1.15	1.17	1.22	1.28
0.10	1.31	1.19	1.16	1.20	1.28	1.42
1.00	1.38	1.24	1.24	1.36	1.53	2.09
10.0	1.57	1.38	1.35	1.46	1.65	1.72
KS	1.69	1.44	1.38	1.53	1.66	1.28

solution and the other with 10^{-2} M serine added to the same solution. Inoculation of the bacteria was identical. Table V lists results of two experiments performed on another day with two different serine concentrations, 10^{-2} M and 10^{-3} M, in the motility buffer. Thus the bottom half of Table IV and the top half of Table V show two similar experiments done on two different occasions, using similar procedures. The difference and similarity between the two results reflects the extent of reproducibility of the experiment. The largest uncertainty probably comes from preparation of the bacteria from day to day. According to previous experiments of Adler (3), all four cases we studied correspond to oxygen-limited situations and therefore the substrate is the oxygen and not the serine. Thus the coefficient D has been set to 2.12×10^{-5} cm^2/s (17) in all calculations.

The "instantaneous" speed we obtained varies from 0.1–1 μm/s. The order of magnitude is correct, as can be seen from the following estimate. According to Eq. 19, the speed of migration is $\bar{v} \doteq (N/A)\,(k/C_o)$. We pointed out in Experimental Procedure that the total number of bacteria inoculated was 1×10^8. From the first picture in Fig. 2, we estimate that 10% of the bacteria inoculated ascend to form the band. Because $A = 1$ cm^2 we have $(N/A) = 1 \times 10^7$/cm^2. If the oxygen consumption rate is taken (10) to be $k = 5 \times 10^{-12}$ mmol/cell h, then using the saturated oxygen concentration in water at room temperature

TABLE IV
COMPARISON OF BACTERIA MIGRATING IN MOTILITY BUFFER CONTAINING NO SERINE AND 10^{-2}M SERINE

Time	$\bar{v}$	$\langle\xi^2\rangle^{0.5}$	$\langle\xi^3\rangle/\langle\xi^2\rangle^{1.5}$	$\langle\xi^4\rangle/\langle\xi^2\rangle^2$	$\bar{\delta}$	μ	μ_{KS}	δ_{KS}
min	*μm/s*	*mm*				$10^{-7}\frac{cm^2}{s}$	$10^{-7}\frac{cm^2}{s}$	
No Serine								
0	0.83 ± 0.04	0.33 ± 0.03	0.56 ± 0.12	1.15 ± 0.09	1.30 ± 0.15	13 ± 1	18 ± 1	1.52 ± 0.12
50	1.08 ± 0.06	0.24 ± 0.02	0.11 ± 0.25	1.22 ± 0.18	2.0 ± 0.45	8.9 ± 1.5	15 ± 1.3	1.91 ± 0.24
117	0.64 ± 0.08	0.25 ± 0.01	−0.06 ± 0.19	1.18 ± 0.08	2.34 ± 0.40	5.6 ± 0.6	8.6 ± 0.6	2.07 ± 0.19
221	0.50 ± 0.04	0.42 ± 0.02	−0.65 ± 0.07	1.51 ± 0.06	4.7 ± 0.30	4.3 ± 0.2	8.9 ± 0.3	2.73 ± 0.13
10^{-2}M Serine								
38	0.28 ± 0.09	0.41 ± 0.04	0.43 ± 0.11	0.95 ± 0.06	1.47 ± 0.15	5.4 ± 0.3	7.4 ± 0.2	1.63 ± 0.10
61	0.89 ± 0.13	0.37 ± 0.04	−0.03 ± 0.25	0.98 ± 0.08	2.28 ± 0.40	12 ± 1.5	18 ± 1.5	2.04 ± 0.20
105	0.75 ± 0.08	0.38 ± 0.03	0.37 ± 0.20	1.15 ± 0.15	1.58 ± 0.30	12 ± 1	17.5 ± 1	1.69 ± 0.20
235	0.09 ± 0.03	0.32 ± 0.01	0.63 ± 0.15	1.21 ± 0.12	1.20 ± 0.20	1.4 ± 0.2	1.9 ± 0.2	1.47 ± 0.20

The origin of time is taken at 1 h after inoculation.

TABLE V
COMPARISON OF BACTERIA MIGRATING IN MOTILITY BUFFER CONTAINING 10^{-2}M SERINE AND 10^{-3}M SERINE

Time	$\bar{v}$	$\langle\xi^2\rangle^{0.5}$	$\langle\xi^3\rangle/\langle\xi^2\rangle^{1.5}$	$\langle\xi^4\rangle/\langle\xi^2\rangle^2$	$\bar{\delta}$	μ	μ_{KS}	δ_{KS}
min	*μm/s*	*mm*				$10^{-7}\frac{cm^2}{s}$	$10^{-7}\frac{cm^2}{s}$	
10^{-2}M Serine								
0	0.32 ± 0.03	0.29 ± 0.01	0.49 ± 0.10	1.08 ± 0.07	1.39 ± 0.14	4.4 ± 0.2	5.9 ± 0.2	1.57 ± 0.09
48	0.50 ± 0.02	0.31 ± 0.02	0.54 ± 0.19	1.16 ± 0.09	1.34 ± 0.24	7.6 ± 0.8	10 ± 0.6	1.53 ± 0.17
87	0.26 ± 0.07	0.33 ± 0.02	0.76 ± 0.20	1.27 ± 0.17	1.05 ± 0.15	4.7 ± 0.5	5.9 ± 0.4	1.37 ± 0.15
218	−0.11 ± 0.09	0.33 ± 0.01	0.24 ± 0.12	1.15 ± 0.10	1.76 ± 0.23	1.4 ± 0.1	2.0 ± 0.1	1.80 ± 0.10
10^{-3}M Serine								
14	0.81 ± 0.03	0.42 ± 0.02	0.45 ± 0.12	0.87 ± 0.03	1.48 ± 0.14	16 ± 0.5	22 ± 0.5	1.60 ± 0.12
31	0.71 ± 0.02	0.57 ± 0.03	0.71 ± 0.11	0.97 ± 0.08	1.09 ± 0.12	22 ± 0.5	27 ± 0.6	1.38 ± 0.10
95	0.41 ± 0.05	0.45 ± 0.04	0.66 ± 0.24	1.05 ± 0.11	1.16 ± 0.25	9.5 ± 1.1	12 ± 1	1.42 ± 0.12
206	0.65 ± 0.09	0.48 ± 0.03	0.30 ± 0.11	0.72 ± 0.02	1.67 ± 0.17	13 ± 0.5	19 ± 0.7	1.74 ± 0.10

The origin of time is taken at 2 h after inoculation.

(10) $C_o = 2 \times 10^{-4}$ mmol/cm^3. Eq. 19 gives for the migration speed $\bar{v} = 0.25$ cm/h or 0.7 μm/s, which is in the measured range.

To compare the profile that is measured in real space scale ξ (millimeters) and the theoretical prediction that is given in a dimensionless scale $x = \bar{v}\xi/\mu$, we proceed as follows.

First, the reduced third central moment of a measured profile, $<\xi^3>/<\xi^2>^{1.5}$ is equated to $<x^3>/<x^2>^{1.5}$ in Fig. 6 (ordinate), and the approximate $\bar{\delta}$ (abscissa) value is determined by an initial choice, $\gamma \simeq 0.05$ say. Next, using the set of parameters $(\bar{\delta}, \gamma)$ obtained this way, we read off a value of $\sqrt{<x^2>}$ from Fig. 5. Then by comparing this value with the experimentally measured value of $\sqrt{<\xi^2>}$, we get the parameter $\mu/\bar{v}$. Because $\bar{v}$ is known from an independent measurement, we have a value for μ. With the value of μ so obtained, we can then improve on our initial estimate by recalculating $\gamma = \mu/D$ using $D = 2.1 \times 10^{-5}$ cm^2/s. With this new value of γ we again go back to Fig. 6 and get a more accurate value of $\bar{\delta}$. This self-consistent procedure can be repeated twice to get the desired $\bar{\delta}$ and μ for each profile measured at a different time and under different conditions. The error indicated in Tables IV and V reflects the combined uncertainties in this procedure. We also list μ_{KS} and δ_{KS} obtained by using the KS analytical solution. In this case there is no parameter γ so the use of an experimental normalized third central moment in Fig. 6 is sufficient to uniquely determine $\bar{\delta}_{KS}$. Then an additional use of a $\sqrt{<\xi^2>}$ datum in Fig. 5 uniquely determines μ_{KS}. We see, however, that μ_{KS} and δ_{KS} so obtained is substantially different from μ and δ.

A further test of the theory can be made by comparing the normalized fourth central moments of the measured and calculated profile. Table III shows that the calculated fourth central moment is rather insensitive to both $\bar{\delta}$ and γ in the range of experimental interest, and is $\simeq$1.2 for our numerical solution and $\simeq$1.4 for the KS. We see from Tables IV and V that the measured values are closer to 1.2, indicating agreement between our numerical solution and experiments.

Finally, a test of the calculated profile itself is made in Fig. 7. This datum corresponds to the one in Table IV at a time of 50 min, for which $\bar{\delta} = 2.0$ and $\mu = 8.9 \times 10^{-7}$ cm^2/s. One

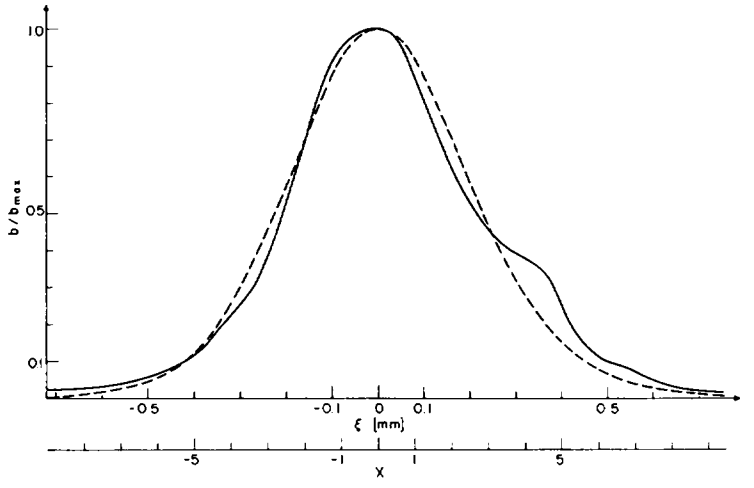

FIGURE 7 Comparison of the band shape predicted by our numerical solution with $\bar{\delta} = 2.0$ (dashed curve) and a measured profile smoothed by the 45-point averaging. The scale factor $\mu/\bar{v}$ that converts the x into the actual distance ξ is 81 μm. This corresponds to $\mu = 8.9 \times 10^{-7}$ cm^2/s and $\bar{v} = 1.1$ μm/s. The experimental data correspond to the one in Table IV at a time of 50 min.

sees that the corresponding theoretical curve calculated with $\bar{\delta} = 2.0$ and $\mu = 8.9 \times 10^{-7}$ cm^2/s agrees quite well with the measured one.

As one can see from Fig. 4, the line shape of $b(x)$ and $b_{KS}(x)$ is not very different. The major difference between them is in the width. $b(x)$ is in general broader than $b_{KS}(x)$ because of the substrate diffusion. Therefore, if we use $b_{KS}(x)$ to fit the experimental data in Fig. 7, we would also get a reasonable fit except the values of μ_{KS} and $\bar{\delta}_{KS}$ so obtained would be substantially different from the corresponding μ and δ as can be seen from Tables IV and V.

Time-Dependent Fine Structure

As already mentioned in the previous sections, an interesting observation, made possible by the rapid-scanning densitometer, is that of the existence of fine structures in the band profile. In the case of oxygen-saturated motility buffer solution, the fine structure is relatively weak, as can be seen from the middle picture in Fig. 3. However, in the solution with serine added, the fine structure becomes quite pronounced and is visibly time-dependent. Fig. 8 shows an example of such a time-dependent fine structure in a 10^{-2} M serine solution. This set of data corresponds to the one at 105 min in Table IV. Starting from the top picture, each following picture represents the successive scan taken at an interval of 50 s. One can discern approximately five narrow peaks superposed on an otherwise smooth band profile over a distance of 1 mm. This makes an average distance between the peaks equal to 200 μm. Moreover, although each fine structure peak seems to stay at about the same location over the time span of 150 s, the peak intensity is visibly different from scan to scan (scan time, 10.5 s).

We shall attempt to understand the occurrence of the fine structure physically as follows. Theoretically, we obtain the time invariant band profile from the simplified Eqs. 9 and 10. To get the fine structure, we have to use the original time-dependent partial differential Eqs. 6 and 7 that govern the densities $b(\xi, \tau)$ and $c(\xi, \tau)$. Starting from a uniform bacterial

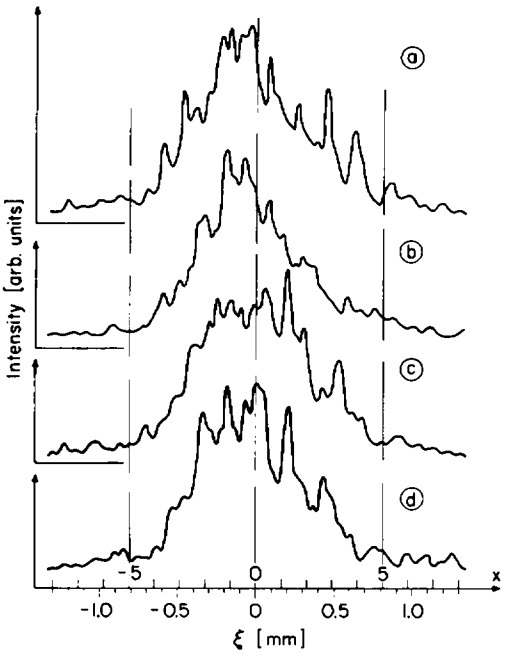

FIGURE 8 An example of the time-dependent fine structures of a migrating band as measured by the rapid-scanning laser densitometer. Successive curves (*a–d*) are recorded at 50-s intervals and are part of the data in Table IV at a time of 105 min. They are aligned with respect to the first moment. (arb. denotes arbitrary)

distribution $B(\xi)$, obtainable from Eqs. 9 and 10, suppose there is a fluctuation of the number of bacteria $b'(\xi, \tau)$ at a certain location. This can be due to an accidental pile-up of a number of bacteria at ξ as a result of their random walks. Because the motility coefficient μ is rather small ($\mu \simeq 1 \times 10^{-6}$ cm^2/s), it takes some time for this density spot to diffuse away. In fact, we can estimate the time constant to be

$$\tau_B \simeq \frac{<(\Delta x)^2>}{2\mu} \simeq \frac{(100 \times 10^{-4})^2}{2 \times 1 \times 10^{-6}} = 50 \text{ s},$$

where we take $\sqrt{<(\Delta x)^2>}$ to be half the average separation between two fine structure peaks. The added bacteria consume extra substrate around ξ to create a dip in $c(\xi, \tau)$. This dip in c increases the magnitude of $-(\partial c/\partial \xi)$ at ξ which further enhances the coupling term

$$-\frac{\delta}{c}\frac{\partial c}{\partial \xi} b.$$

Eq. 6 then, shows a net increase of $b(\xi, \tau)$ in time. This is a positive feedback effect that tends to build up the bacterial density around a spot ξ once there is an accidental fluctuation there. However, the buildup of bacteria would not continue indefinitely. Eventually, the substrate diffusion would even up the dip created by the bacteria. This time constant can be estimated

to be

$$\tau_D \simeq \frac{<(\Delta x)^2>}{2D} \simeq \frac{(200 \times 10^{-4})^2}{2 \times 2 \times 10^{-5}} = 10 \text{ s}.$$

Thus the characteristic time of the build-up is of the order of 10 s, and after that, the bacteria gradually move away from the local maximum in a characteristic time of $\simeq$50 s. Data shown in Fig. 8 are not inconsistent with this intuitive picture. For an accurate prediction of the spatial and temporal structures, we have to perform linear and nonlinear stability analyses of Eqs. 6 and 7 (19). Because they involve substantial numerical analysis we have not had a chance to pursue them yet. Until such analyses are completed our physical argument presented above remains tentative.

CONCLUSIONS

We have demonstrated experimentally that the Keller-Segel model describes reasonably well the migration and the density profile of the chemotactic bands of *E. coli* in motility buffer with or without serine. In the oxygen-limited cases that we have studied, it is important to take into account the diffusion of the substrate to obtain a quantitative measurement of μ and δ. We describe a convenient procedure by which a unique set of values of μ and δ can be extracted, given an independent measurement of $\bar{v}$. In a solitary wave approximation, where we neglect the time dependence of $b(\xi, \tau)$, the migration speed $\bar{v}$ is strictly constant. The experimental fact that $\bar{v}$ cannot be regarded as constant over a period longer than $\simeq$10 min indicates that the solitary wave approximation is valid only over a period of $<$10 min. Over a longer period of time when there is significant change in the profile, as evidenced by the change of μ and δ values, the speed $\bar{v}$ also changes. There should also be a connection between the speed variation over a shorter time and the variation of the fine structure over the same period of time. Therefore, in an approximate sense, the measurements listed in each row of Tables IV and V can be regarded as an independent situation. Compounded to this mathematical complication of the KS model, it is also possible that each parameter in the model, k, μ, and δ, has its own time dependence due to biological reasons. This aspect of the problem is beyond the scope of this paper. Our main finding is that μ generally lies in the range $1\text{–}10 \times 10^{-7}$ cm^2/s and the ratio δ:μ in the range 1.1–2.5.

The measured value of $\bar{\delta}$ can be used to clarify a loose statement made in the introduction that "the bacteria collectively seek a certain optimum oxygen concentration within a traveling oxygen gradient. . . ." In view of Eq. 17 the so-called optimum oxygen concentration should be replaced by the "optimum logarithmic derivative of the oxygen concentration distribution." Thus a physical meaning of the parameter $\bar{\delta}$ is that its inverse defines the value of the optimum logarithmic derivative of the oxygen concentration distribution.

We would like also to note that the parameter μ measured in this experiment, aside from its obvious meaning of a diffusion coefficient measuring the random motility of the bacteria, can be combined with results from a quasi-elastic light scattering experiment (9) to further extract the microscopic parameters t_1 and t_2 mentioned in the Introduction. Using a simple kinetic theory argument (20) one can show:

$$\mu = \frac{1}{3}\frac{u^2}{1 - \overline{\cos\theta}}\frac{1}{\nu}, \tag{32}$$

where u^2 is the mean square speed of the "run," ν the frequency of change of direction (collision), and $\overline{\cos\theta}$ the mean cosine of the persistence angle from one run to another. If there were negligible time spent on twiddle then $\nu = t_1^{-1}$, as the situation in a simple gas. However, because we know (9) there is an appreciable amount of twiddle, a correct way to take into account presence of t_2 is to put

$$\nu = \frac{1}{t_1} + \frac{1}{t_2} \tag{33}$$

From our previous light-scattering experiment (9) we get $u = 22\ \mu m/s$. If we take $\overline{\cos\theta} = \cos 65° = 0.42$ as was observed by Berg and Brown (4), then using a typical value $\mu \simeq 1 \times 10^{-6}\ cm^2/s$ we get from Eq. 32 $\nu^{-1} = 0.36$ s. Also from the light-scattering experiment (9) we can estimate $t_2/(t_1 + t_2) \equiv \beta$. Using a spherical particle approximation we obtained $\beta = 0.67$, which, as we already commented (9), is too large an estimate. If we take into account the nonsphericity of *E. coli* and also its wobble motion (21) during the run, we would obtain β as low as 0.4. For the sake of argument here, let us take a reasonable mean value $\beta = 0.5$, or $t_1/t_2 = 1$. Then using $\nu^{-1} = 0.36$ and Eq. 33 we get $t_1 = t_2 = 0.72$ s. In view of the high bacterial density inside the band ($b \simeq 1 \times 10^8$ bacteria/cm^3) such values of t_1 and t_2 seem quite reasonable.

As for the newly found fine structure, it would be very interesting to study the spatial as well as the temporal structures as a function of concentration of various chemotactic agents. We already observed a drastic change in the magnitude of the fine structure as the serine concentration goes below 10^{-4} M. Mathematically we must perform a linear stability analysis of Eqs. 6 and 7 to find out the region of instability and also the wavenumber range where the instability occurs. Ultimately, we will have to study correlation function of the type $<b(\xi_1, \tau_1)\, b(\xi_2, \tau_2)>$ as a function of the critical parameters. With the rapid-scanning technique we can obtain essentially the "instantaneous" profile, from which we can compute such a correlation function. Because the instability is believed to be due to the nonlinear coupling term between the bacterial density and the substrate concentration gradient, the detailed study of the instability should shed further light on the form of the coupling term. Thus the study of the fine structure may eventually add to our understanding of the chemotaxis itself.

The authors wish to acknowledge fruitful conversations with Professor Tom Chang on the subject of stability analysis. Many constructive criticisms of the referees which helped to clarify the presentation are also appreciated.

Research for this paper was supported by a Sloan Fund for Basic Research and National Institutes of Health Biomedical Research Support grant to the Massachusetts Institute of Technology and the National Science Foundation.

Received for publication 14 July 1978 and in revised form 18 December 1979.

REFERENCES

1. BEYERINCK, M. W. 1893. Ueber Atmungsfiguren beweglicher Bakterien. *Zentr. Bakteriol. Parasitienk.* **14**:827.
2. ADLER, J. 1966. Chemotaxis in bacteria. *Science (Wash. D.C.).* **153**:708.
3. ADLER, J. 1966. Effect of amino acids and oxygen on chemotaxis in *Escherichia coli*. *J. Bacteriol.* **92**:121.

4. BERG, H. C., and D. A. BROWN. 1972. Chemotaxis in *Escherichia coli* analyzed by three-dimensional tracking. *Nature (Lond.)*. **239**:500.
5. MACNAB, R. M., and D. E. KOSHLAND, JR. 1972. The gradient sensing mechanism in bacterial chemotaxis. *Proc. Natl. Acad. Sci. U.S.A.* **60**:2509.
6. ADLER, J. 1975. Chemotaxis in bacteria. *Annu. Rev. Biochem.* **44**:344.
7. BERG, H. C. 1975. Chemataxis in bacteria. *Annu. Rev. Biophys. Bioeng.* **4**:119.
8. KOSHLAND, D. E., JR. 1977. A response regulator model in a simple sensory system. *Science (Wash. D.C.)* **196**:1055.
9. HOLZ, M., and S-H. CHEN. 1978. Quasi-elastic light scattering from migrating chemotactic bands of *Escherichia coli*. *Biophys. J.* **23**:15.
10. KELLER, E. F., and L. A. SEGEL. 1971. Traveling bands of chemotactic bacteria: a theoretical analysis. *J. Theor. Biol.* **30**: 235.
11. WHITHAM, G. B. 1974. *Linear and Non-Linear Waves*. John Wiley & Sons, Inc., New York. Wiley-Interscience Div.
12. NOSSAL, R., and S-H. CHEN. 1973. Effects of chemoattractants on the motility of *Escherichia coli*. *Nat. New Biol.* **244**:253.
13. CHANDRASEKHAR, S. 1943. Stochastic problems in physics and astronomy. *Rev. Mod. Phys.* **15**:57.
14. DAHLQUIST, F. W., P. LOVELY, and D. E. KOSHLAND. 1972. Quantitative analysis of bacterial migration in chemotaxis. *Nat. New Biol.* **236**:120.
15. SCRIBNER, T. L., L. A. SEGEL, and E. H. ROGERS. 1974. A numerical study of the formation and propagation of traveling bands of chemotactic bacteria. *J. Theor. Biol.* **46**:189.
16. SCOTT, A. C., F. Y. F. CHU, and D. W. MCLAUGHLIN. 1973. Solitons—a new concept in applied physics. *Proc. IEEE*. **61**:1443.
17. MCCABE, M., and T. V. LAURENT. 1975. Diffusion of oxygen, nitrogen and water in hyaluronate solutions. *Biochim. Biophys. Acta*. **399**:131.
18. CONTE, S. D. 1965. Elementary Numerical Analysis. McGraw-Hill Book Co., New York.
19. NICOLIS, G., and I. PRIGOGINE. 1977. Self-Organization in Non-Equilibrium System—From Dissipative Structures to Order Through Fluctuations, John Wiley & Sons, Inc., New York.
20. LOVELY, P. S., and F. W. DAHLQUIST. 1975. Statistical measures of bacterial motility and chemotaxis, *J. Theor. Biol.* **50**:477.
21. HOLZ, M., and S-H. CHEN. 1978. Rotational-translational models for interpretation of quasi-elastic light scattering spectra of motile bacteria. *Appl. Opt.* **20**:3197.